

Twisted Pair Transmission Line Coil- A Flexible, Self-Decoupled and Extremely Robust Element for 7T MRI

Jules Vliem¹, Ying Xiao^{2,3}, Daniel Wenz^{2,3}, Lijing Xin^{2,3}, Irena Zivkovic^{1*}

¹Eindhoven University of Technology, Electrical Engineering Department, Eindhoven, Netherlands

²CIBM Center for Biomedical Imaging, Lausanne, Switzerland

³Ecole Polytechnique Federale de Lausanne (EPFL), Animal Imaging and Technology, Lausanne, Switzerland

*Corresponding author: Irena Zivkovic, i.zivkovic@tue.nl

1. Introduction

There has been ongoing research on developing highly flexible RF coil arrays that can adapt to fit a variety of patients [1-6]. Since their flexible and tight fit nature, transmit and receive performances of those arrays are maximized. Interelement decoupling is very important parameter in mentioned arrays. Not sufficient decoupling between the elements decreases performances of the array. Various methods are used for element decoupling such as partial overlapping [7], capacitive and inductive networks [8-10], transformer decoupling [11] and use of strategically placed passive resonators [12, 13]. When preamplifier is used for decoupling [7] it limits the coil functioning to receive only modality. In terms of decoupling, the ideal coil element would be truly self-decoupled element which, when placed in an array configuration, would stay decoupled from the other elements without additional application of any decoupling technique. Proposed shielded-coaxial-cable (SCC) coil exhibits highly decoupled nature per se - it is demonstrated that placing of SCC elements in various array configurations keeps elements highly decoupled which allowed high performance imaging at 7T [1, 15].

In this manuscript, we are proposing a coil element made by modification of the twisted pair transmission line. The coil concept is very similar to SCC coil design – twisted pair transmission line was initially circularly shaped and, to ensure transmission (also reception) of the electromagnetic fields, one conductor was interrupted at the top of the coil (while being continuous at the opposite point) while the other conductor was continuous at the top and interrupted at the bottom (opposite) point to enable its connection to the tuning and matching circuit. This coil design demonstrated improved flexibility and robustness towards the elongation and shape deformation without need for re-tuning and allowed high interelement decoupling when placed in an array configuration. Previous studies have explored the use of the twisted pair loop as receive only elements in both 3T [4, 5] and 7T [6] MRI systems. In those abstracts, decoupling properties, SAR and transmission efficiencies and robustness of the coil were not investigated in detail since the coil was used as receive only element.

In this paper, we compared twisted pair coil with conventional one in terms of B_1^+ field efficiency, maximum SAR, robustness towards elongation and shape changes and interelement decoupling when

placed in various arrays. It showed stable both S_{11} and maximum SAR_{10g} , which allows use of the coil which is tuned and matched only once.

2. Methods

2.1 The main coil concept

To create the twisted pair loop coil, two polytetrafluoroethylene (PTFE) insulated copper wires are twisted around one another (Figure 1(a)), creating a flexible structure. The twisted wire is shaped into a loop and gaps are introduced for both wires, as illustrated in Figure 1(b). The cut in the grey wire (referred to as the "shield wire") at the top, opposite of the feeding point, effectively un-shields the magnetic field, making the coil sensitive to electro-motive forces (EMF) and thus resonant. At the feeding point, a cut is made in the complementary red wire (referred to as the "signal wire") to facilitate interfacing with the MRI scanner, enabling the transmission and reception of signals.

2.2 Simulation based design of the twisted pair coil

The initial step in our design process involves determining the optimal twisting density per unit length for the wires. The twisted pair coil was modelled using SolidWorks (Dassault Systèmes SolidWorks Corporation, Waltham, USA) and imported in CST Studio Suite 2023 (Dassault Systèmes, Vélizy-Villacoublay, France). The twisted pair is modelled by drawing two circles with 1mm diameter, representing the copper conductor, spaced 2 mm apart. These circular profiles are swept along a predefined path, which can be circular or of arbitrary shape, to create the coil. All models have a total length or circumference of 31.4 cm and are shaped into circular, elongated, or arbitrary forms. Cuts of 2 mm are introduced at the specified locations for both wires mentioned earlier. A discrete port is connected between the gaps at the feed point (red "signal wire"). Lumped elements are added to the port in the schematic tab to achieve coil tuning and matching at 297.2 MHz to 50 Ω .

To accurately mesh the complex geometry of the twisted shape, tetrahedral meshing is preferred. Tetrahedral meshing enables rapid and accurate meshing of intricate curved geometries compared to hexahedral meshing, which would not accurately capture the twisted and curved structure [15]. Therefore, the frequency domain solver with tetrahedral meshing is employed, utilising adaptive mesh refinement with a minimum of 3 and a maximum of 8 passes. The simulations are conducted by placing a coil on a homogeneous cubic phantom ($\epsilon_r = 68$, $\sigma = 0.48$ S/m, dimensions 40 x 40 x 40 cm), Figure 3(c)), with the coils positioned at 2 cm distance from the phantom. The copper cores are modelled as annealed copper, while the insulation of both wires is excluded due to meshing issues and its negligible impact on the simulation results. All the simulation results were scaled to 1 W of accepted power.

To investigate the optimal number of twists per length, we looked at various performance metrics on the cubic phantom, including the transmit efficiency (B_1^+) at a 5cm depth in the phantom, maximum Specific Absorption Rate ($\max SAR_{10g}$), SAR efficiency at 5cm depth (B_1^+ divided by the square root of the maximum SAR_{10g}) and the coil's robustness towards the elongation (from circular shape to medium

and extremely elongated shapes). We observed mentioned parameters for coils designed with different number of twists per coil length, such as 10, 24, 48 and 64 twists per 31.4 cm (the circumference of all coils) and for different elongations. The robustness analysis involved comparing the return loss (S_{11}) of the tuned and matched circular coil and utilising the same circuitry for the elongated coil.

To compare the performance of the twisted pair loop coil we conducted a comparison with a conventional loop coil featuring distributed capacitors (Figure 3(b)) on a cubic phantom. We compared the performance in terms of robustness (S_{11}), B_1^+ field strength, and maximum SAR_{10g} for the two coils under both circular and elongated configurations. The copper loop was modelled as a 10 cm diameter loop, constructed using 1 mm thick copper wire.

To demonstrate the extraordinary flexibility of the twisted pair loop coil, we further expanded its design by modelling it as a spline shape. This approach allowed us to create diverse and intricate coil configurations by defining arbitrary splines in SolidWorks and sweeping the circular profiles along the spline path. The coil was tuned and matched at the beginning in circular shape (diameter 10 cm, circumference 31.4 cm) and subsequently, the shape was deformed while keeping the same tuning and matching circuit elements. We present two examples of the twisted pair spline configurations in Figure 8(a) and (b). To assess the coil's consistent performance, we again evaluated its robustness (S_{11}), B_1^+ field strength, and SAR characteristics.

2.3 Coil Construction

The twisted pair coil is constructed by tightly twisting two 18-gauge wires (1 mm diameter) with PTFE insulation. To achieve a higher number of twists per length, a recommended method is to cut two large sections of wire and secure one end in a bench vise. The other end of the wires is inserted into a drill, and by turning the drill, the wires are twisted while maintaining tension by gently pulling them. The maximum twists per length is reached when the wires become significantly taut. At this point, the twisted pair can be removed from the vise and drill. Twisted pair coils which we fabricated had 64 twists per coil length (length = circumference 31.4 cm).

Before connecting the loop to the circuitry, a cut is made in the middle of the grey shield wire. The size of this cut affects the coil's tuning, where a larger cut slightly lowers the resonance frequency. The grey shield wire cuts were approximately 2 mm in our construction. The coil's physical realisation and its corresponding schematic are shown in Figure 3(a). The coil, with a diameter of 10 cm, is tuned and matched using one parallel and two series fixed capacitors (AVX800 E Series, Kyocera-AVX, Fountain Inn, USA). The red signal wire is attached to both sides of the parallel capacitor, while the grey shield wires are connected, either twisted or soldered on the same trace of the PCB. The PCB is created by milling signal traces on a copper plated FR4 material. Two series capacitors are added after the parallel capacitor, and the circuitry is fed by an RG58 coaxial cable (RG58 LSZH, Multicomp PRO, London, UK).

To compare the performance of the twisted pair loop coil, a conventional copper loop was also fabricated, as depicted in Figure 3(b) along with its circuitry. The conventional coil is constructed using a copper wire with a wire diameter of 1 mm. Fixed and variable capacitors are distributed along the 100 mm diameter loop, and one parallel and two series fixed capacitors are utilised for tuning and matching the coil at 297.2 MHz.

2.4 Bench and MRI Measurements

2.4.1 S-parameter measurements

The individual elements were assessed on a cubic phantom (See Figure 3(c)), placed 2 cm away from the phantom using a foam spacer. S-parameters were measured with a Vector Network Analyser (VNA) (Keysight N9914A FieldFox VNA 6.5GHz) for individual elements and when placed in an array configuration.

To investigate the coupling behaviour (S_{21}) of the twisted pair coil, two elements were placed in proximity. The distance between the elements was systematically adjusted, starting from 20 mm apart and gradually reducing the separation until they overlapped by 90 mm (90% of the coil's diameter). Furthermore, a different orientation configuration was tested (as depicted in Figure 6 (a)), while varying the overlapping distance from 0 mm up to 50 mm. Also, here the overlapping distance was varied (from 0 mm to 50 mm).

In addition to the individual and two element measurements, we conducted S-parameter measurements on three different array configurations, as shown in Figure 7.

2.4.2 MRI measurements

The spherical phantom experiments were performed on a 7T MR human scanner (Magnetom, Siemens Healthineers, Erlangen, Germany). The three-dimensional B_1^+ maps were quantitatively measured with SA2RAGE sequence (TR/TE = 2400/0.78 ms, $T_1/T_2 = 45/1800$ ms, $\alpha_1/\alpha_2 = 4^\circ/10^\circ$, FOV = 208×256 mm², slices = 64, resolution = $2.0 \times 2.0 \times 2.5$ mm³, BW = 1220Hz/px, scan time = 115 s) [16]. To get the resulting data to the same units as the simulated B_1^+ we used:

$$B_1^+ = \frac{\text{Pixel Value} \cdot B_1^+ \text{ Scaling}}{\text{Pixel Intensity}}$$

where *Pixel Value* is the pixel data from the scanner, $B_1^+ \text{ Scaling}$ is the value of the B_1^+ field corresponding to a specific *Pixel Intensity*. Here the $B_1^+ \text{ Scaling} = 11.73 \mu\text{T}$ for a *Pixel Intensity* of 1000. The B_1^+ results obtained from the experiments were subsequently normalised to the input power.

3. Results

3.1 Individual coil design and comparison with conventional element

In Figure 2 (a) simulated S_{11} of the coils made of twisted pair transmission line with different number of twists per circumference length. The coils were tuned and matched in circular shape and then S_{11} was monitored when they were elongated. Examined number of twists per circumference length were 10, 24, 48 and 64. The S_{11} of the coil with the highest number of twists per diameter length (64) does not show any changes in S_{11} when elongated. In further work/results, the twisted pair coil with 64

twists per diameter length was used. For a reference, Figure 2(b) shows simulated B_1^+ efficiency at 5 cm depth, maximum SAR_{10g} and SAR efficiency for all examined twisted pair coils with different number of twists. SAR efficiency of elongated coils is lower than efficiency of circular coils while B_1^+ field efficiency of circular shapes was slightly lower than that of elongated. Maximum SAR_{10g} was the lowest for coil with 64 twists per diameter length both in circular and elongated shapes.

Figure 4 shows comparison of B_1^+ field efficiency, maximum SAR_{10g} and SAR efficiency, and S_{11} of twisted pair and conventional coils when the shape changes from circular to medium and extremely elongated. S_{11} of twisted pair coil did not change when the coil was elongated while the conventional coil was very sensitive to elongations. Simulated B_1^+ fields of twisted pair and conventional coils were very similar. Maximum SAR_{10g} simulations reveal that for a twisted pair coil in circular shape it was 1.1W/kg and decreased to 1W/kg in two elongated shapes. Conventional coil had maximum SAR_{10g} of 1.1 W/kg in circular shape while SAR increased to 1.4 W/kg in the maximum elongated shape.

Figure 4(d) shows plotted SAR efficiencies for all examined coils, and they are very similar for both twisted pair and conventional elements. The SAR efficiency is only higher at the superficial depths for elongated coils (both twisted pair and conventional) while after ~2 cm all profiles are very similar.

Figure 5 shows simulated and measured B_1^+ profiles (sagittal and axial slices) of twisted pair coil on a spherical phantom in 3 different shapes – circular, medium and extremely elongated. There is in general very good agreement between simulations and measurements.

3.2 Coupling evaluation of two-element arrays

Figure 6 shows measured coupling between two coils in different amount of overlap and when they were rotated with respect to each other. In all examined cases, decoupling between the two elements was around -15dB. Figure 6(b) shows measured coupling of two elements when the distance between them varies from 20 mm apart to 90 mm of overlap (almost 100% overlap). At all amounts of overlap the measured S_{21} was around -15dB and better. Figure 6(c) shows measured coupling between the two coils when they are rotated for some angle with respect to each other. The highest interelement coupling was noted when the coils were rotated for 180° with respect to each other (yellow line) and it was around -15dB. In the other two examined cases decoupling was way below -20dB.

3.3 Interelement coupling evaluation of multichannel arrays

Figure 7 shows measured interelement coupling of three array configurations made with fabricated coils. All fabricated coils were tuned and matched on a tissue mimicking phantom only once and were placed in an array configuration without further changes in tuning and matching circuits. Figure 7(a) shows 8-channel array consisting of two times four channels with overlapped neighbouring and elements between the two rows. Figure 7(b) shows 8-channel array with overlapped elements between two rows while neighbouring elements within a row were slightly elongated and not overlapped. Figure 7(c) shows elongated non-overlapped elements. In all presented cases S_{11} of individual elements as well as interelement decoupling had excellent performance.

3.4 Evaluation of spline twisted pair transmission line coils

Figure 8 shows two spline twisted pair coil shapes. Coils were tuned and matched at circular shape and subsequently their shapes were deformed without detuning the coils (Figure 8(c)). Those two spline shaped coils were examined for interelement coupling when placed at various distances and various overlaps (Figure 8(d)). They stayed decoupled ($< -15\text{dB}$) in any amount of overlap. B_1^+ field of spline shaped coils followed the coil shape in transversal view (Figure 8(e)). Maximum SAR_{10g} of the first spline “saddle shaped” coil slightly increased to 1.2W/kg (compared to circular shape) while the maximum SAR_{10g} of the second spline “triangular shaped” coil was the same as one of circular shape (1.1 W/kg).

4. Discussion

As results show in Figure 2, a higher number of twists per length, such as 64, yielded a more robust element with lower maximum SAR and similar efficiency in comparison to a lower number of twists per length, such as 10. That was a reason why, both in simulations and experiments, we decided to use the twisted pair coils with 64 twists per chosen circumference of 31.4 cm (10 cm diameter).

In presented work, we examined properties of twisted pair transmission line coil in terms of **B_1^+ field efficiency, maximum SAR_{10g} and interelement decoupling**. By examining these metrics, we gained insights into the coil's ability to maintain its performance across different spline shapes, highlighting its versatility and reliability in practical array configurations.

All simulated and fabricated coils were tuned and matched only once and S_{11} was stable while being elongated, deformed and placed in an array configuration.

In terms of **B_1^+ field efficiency**, the coil has very similar performances compared to the conventional coil of the same diameter (with distributed capacitors). Insensitivity on coil shape deformation is the biggest advantage of this coil compared to conventional design.

Regarding **maximum SAR_{10g}** , in circular form both twisted pair and conventional coils had the same SAR_{10g} of 1.1 W/kg . In elongated forms, twisted pair coils showed decreased SAR from 1.1 W/kg to 1 W/kg , while SAR of conventional coils increased by 40% at maximum elongation. Deformation of twisted pair coil to various *spline* shapes produced minimal increase of SAR (1.1 W/kg and 1.2 W/kg , for two example shapes). The conclusion is that twisted pair coil poses a stable SAR also when shapes deviate from the circular shape while SAR of conventional coil increased by changing shape from circular to elongated. The SAR stability makes twisted pair transmission line coil element a suitable candidate for tight fit, reconfigurable and modular arrays where the coil is potentially exposed to shape changes.

When examined in terms of **interelement decoupling properties**, twisted pair coil showed true self-decoupled nature – it stayed decoupled (better than -10 dB) in all examined array configurations without a need for additional decoupling techniques. It is shown that even in extreme coil shape deformations (spline coil shapes shown in Figure 8), the S_{11} and SAR of individual coil are stable, and they are sufficiently decoupled when placed at various distances from each other. Such superior decoupling properties make twisted pair transmission line coil suitable element for densely populated

receive arrays. This leads to the idea to optimize the shape of the coil when placed in receive array configuration in such a way so to allow high accelerations and maximally improved g-factor.

5. Conclusion

We presented a coil design based on a modified twisted pair transmission line. All simulated and fabricated coils were tuned and matched only once and did not de-tune while being elongated, deformed and placed in array configuration. The coil showed extremely robust performances and stayed decoupled when placed in various array configurations. Proposed element is true self-decoupled element since it is decoupled per-se without need for any additional decoupling technique to be applied. Since the proposed element can properly function when the shape is deformed from circular, future work would include investigation of the optimum shape and arrangement of the coil elements which would allow high accelerations with the best performances.

References

- [1] Ruytenberg, T., Webb, A., and Zivkovic, I. (2020). Shielded-coaxial-cable coils as receive and transceive array elements for 7T human MRI. *Magnetic Resonance in Medicine*, 83(3):1135–1146.
- [2] van Leeuwen, C. C., Steensma, B. R., Klomp, D. W., van den Berg, C. A., and Raaijmakers, A. J. (2022). A fully flexible coaxial cable dipole antenna with flattened current distribution for body imaging at 7 Tesla, *Magnetic Resonance in Medicine*, 87(1):528–540.
- [3] Nohava, L., Czerny, R., Roat, S., Obermann, M., Kuehne, A., Frass-Kriegl, R., Felblinger, J., Ginefri, J. C., and Laistler, E. (2021). Flexible Multi-Turn Multi-Gap Coaxial RF Coils: Design Concept and Implementation for Magnetic Resonance Imaging at 3 and 7 Tesla. *IEEE Transactions on Medical Imaging*, 40(4):1267–1278
- [4] Maravilla, J. A., Gopalan, K., Arias, A. C., and Lustig, M. (2022). Transmission Line Receiver Coils (TLCs) for MRI. In: Proceedings of the 30th scientific meeting, International Society for Magnetic Resonance in medicine, London, p 0189
- [5] J. Maravilla, J. A., Gopalan, K., Arias, A. C., and Lustig, M. (2023). 15-Channel Head Cap Array using Twisted-Pair Elements for MRI,” In: Proceedings of the 31st scientific meeting, International Society for Magnetic Resonance in medicine, Toronto, p 3733
- [6] Czerny, R., Frass-kriegl, R., Cap, V., Laistler, E., and Nohava, L. (2023). Twisted pair coils as flexible receive elements for 7 T - SNR and active detuning efficiency. In: Proceedings of the 31st scientific meeting, International Society for Magnetic Resonance in medicine, Toronto, p 3730
- [7] Roemer, P. B., Edelstein, W. A., Hayes, C. E., Souza, S. P., & Mueller, O. M. (1990). The NMR phased array. *Magnetic resonance in medicine*, 16(2), 192–225.
- [8] Zhang, X., & Webb, A. (2004). Design of a capacitively decoupled transmit/receive NMR phased array for high field microscopy at 14.1T. *Journal of magnetic resonance*, 170(1), 149–155.

- [9] Bilgen M. (2006). Inductively-overcoupled coil design for high resolution magnetic resonance imaging. *Biomedical engineering online*, 5, 3.
- [10] Lee, R. F., Giaquinto, R. O., & Hardy, C. J. (2002). Coupling and decoupling theory and its application to the MRI phased array. *Magnetic resonance in medicine*, 48(1), 203–213.
- [11] Shajan, G., Kozlov, M., Hoffmann, J., Turner, R., Scheffler, K., & Pohmann, R. (2014). A 16-channel dual-row transmit array in combination with a 31-element receive array for human brain imaging at 9.4 T. *Magnetic resonance in medicine*, 71(2), 870–879.
- [12] Avdievich, N. I., Pan, J. W., & Hetherington, H. P. (2013). Resonant inductive decoupling (RID) for transceiver arrays to compensate for both reactive and resistive components of the mutual impedance. *NMR in biomedicine*, 26(11), 1547–1554.
- [13] Yan, X., Zhang, X., Feng, B., Ma, C., Wei, L., & Xue, R. (2014). 7T transmit/receive arrays using ICE decoupling for human head MR imaging. *IEEE transactions on medical imaging*, 33(9), 1781–1787.
- [14] Ruytenberg, T., Webb, A., & Zivkovic, I. (2020). A flexible five-channel shielded-coaxial-cable (SCC) transceive neck coil for high-resolution carotid imaging at 7T. *Magnetic resonance in medicine*, 84(3), 1672–1677.
- [15] Shepherd, Jason & Johnson, Chris. (2008). Hexahedral Mesh Generation Constraints. *Engineering Computers (London)*. 24. 195-213.
- [16] Eggenschwiler, F., Kober, T., Magill, A. W., Gruetter, R., & Marques, J. P. (2012). SA2RAGE: a new sequence for fast B1+ -mapping. *Magnetic resonance in medicine*, 67(6), 1609–1619.

Figures

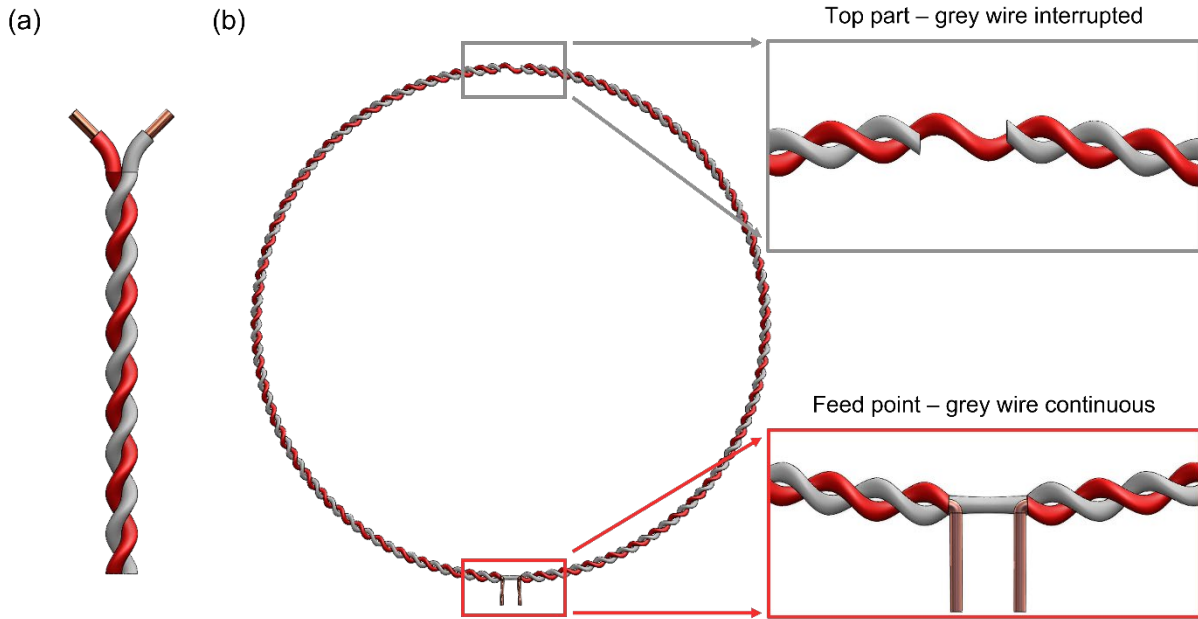


Fig. 1 (a) Illustration of the cables used to make the twisted pair transmission line coil. (b) Forming of the twisted pair coil. A gap is introduced in the grey wire at the top ("shield wire") to un-shield the magnetic field. In the red wire ("signal wire") a gap is introduced at the feeding point (bottom).

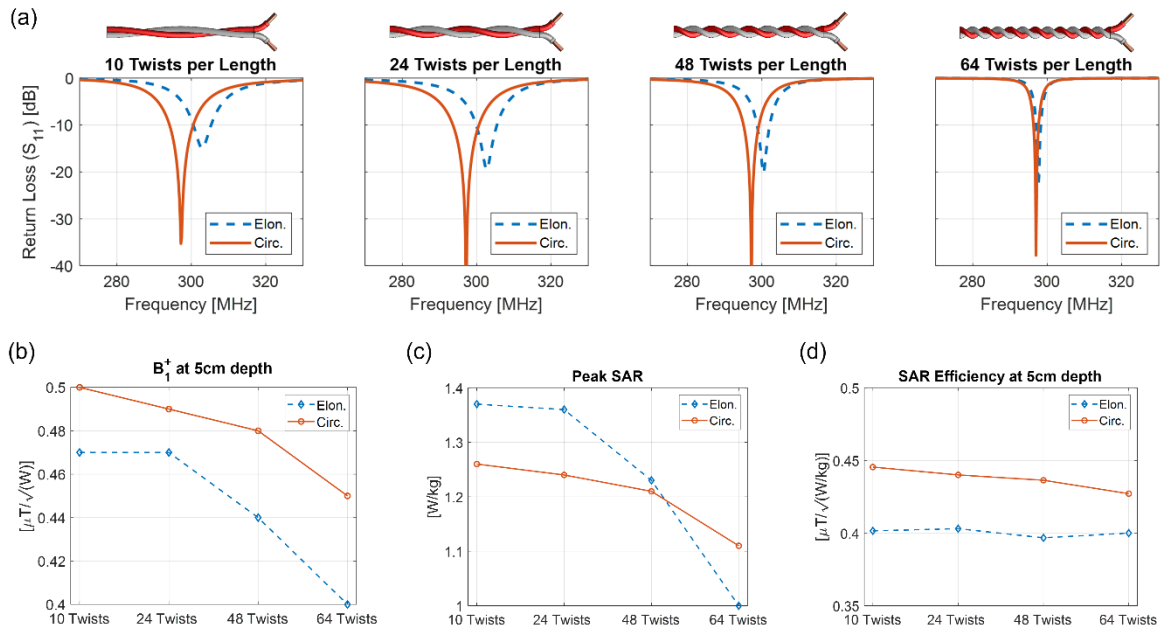


Fig. 2 Simulated metrics of interest for the twisted pair coil with different twist densities. (a) Return loss (S_{11}), in dB, for the tuned and matched circular coil (10cm diameter) and using the same circuitry for the elongated coil ($W \times H = 6 \times 13$ cm). (b) B_1^+ magnitude, in $\mu T/\sqrt{W}$, under the center of the coil, at 5cm depth in the phantom. (c) Peak SAR value, in W/kg, over the phantom. (d) SAR efficiency: B_1^+ magnitude at 5cm depth divided by the square root of peak SAR, in $\mu T/\sqrt{W/kg}$. All results were normalised to 1 W accepted power.

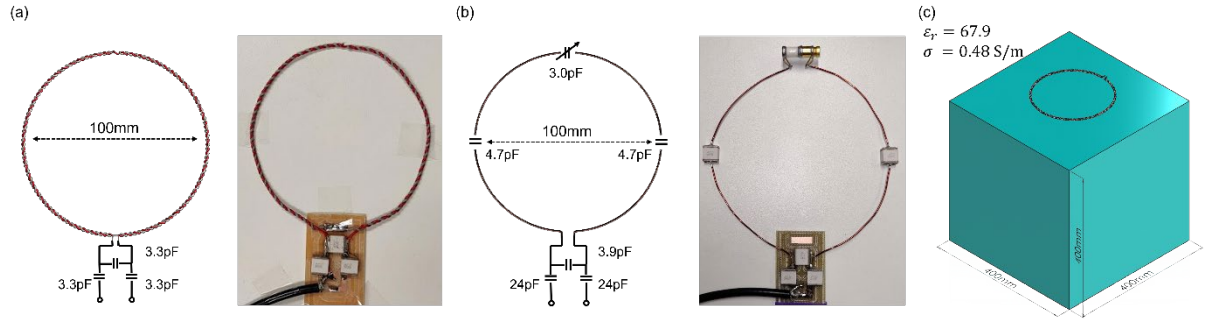


Fig. 3 Schematics and photos of (a) twisted pair loop coil and (b) conventional loop coil. (c) Homogeneous cubic phantom used in simulations and bench measurements. The coil was placed 2 cm away from the phantom.

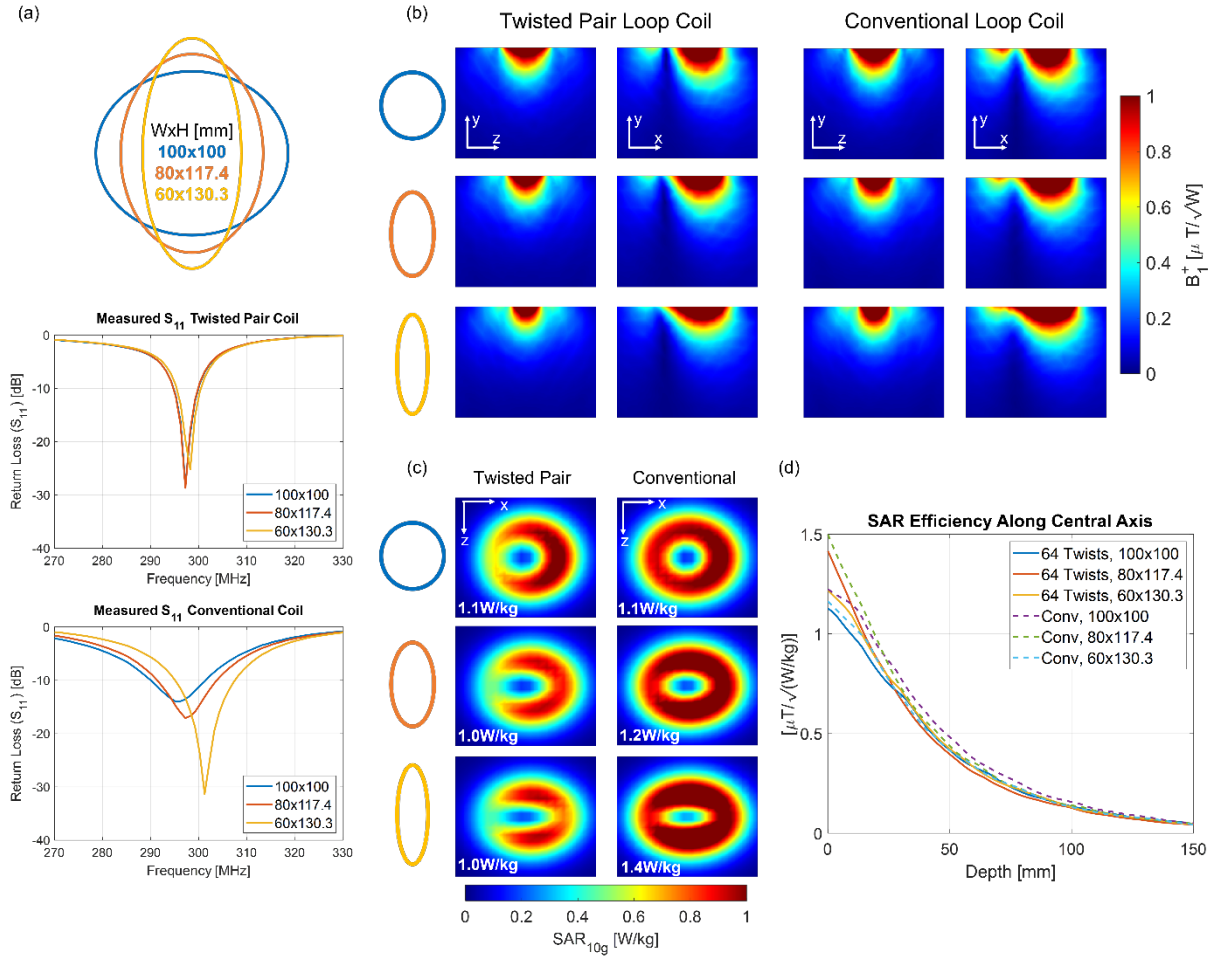


Fig. 4 Comparison metrics for the twisted pair and conventional loop coil, for different amounts of elongation. (a) Measured return Loss (S_{11}), in dB. (b) Simulated B_1^+ field patterns, in $\mu\text{T}/\sqrt{\text{W}}$, on the sagittal and axial plane. (c) Coronal view SAR maps, in W/kg , with its corresponding peak SAR value. (d) SAR efficiency: B_1^+ divided by the square root of peak SAR, in $\mu\text{T}/\sqrt{\text{W/kg}}$, along the central axis of the phantom. All simulated results were normalised to 1 W accepted power.

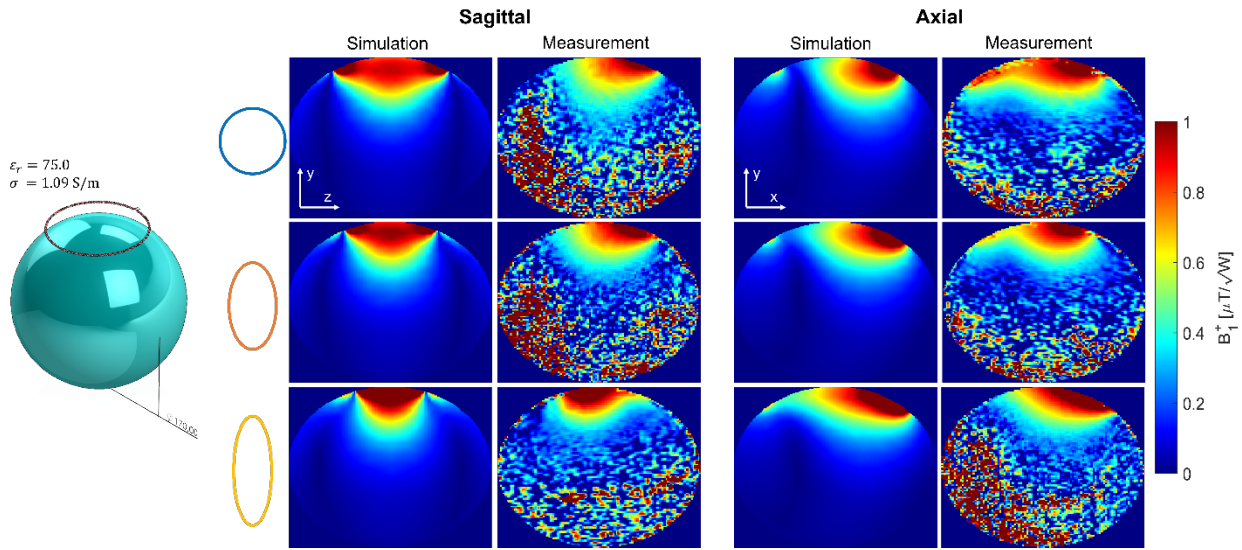


Fig. 5 Simulated and measured B_1^+ maps, in $\mu T/\sqrt{W}$ on both the sagittal and axial planes of a spherical phantom, shown on the left side. The twisted pair coil was tested with varying amounts of elongation, where the elongated coils conformed to the surface of the sphere while maintaining a constant distance of 5mm from the phantom. The simulated results were normalised to 1 W of accepted power and take 25% loss of the experiment into account, while the measurements were normalised to the input power.

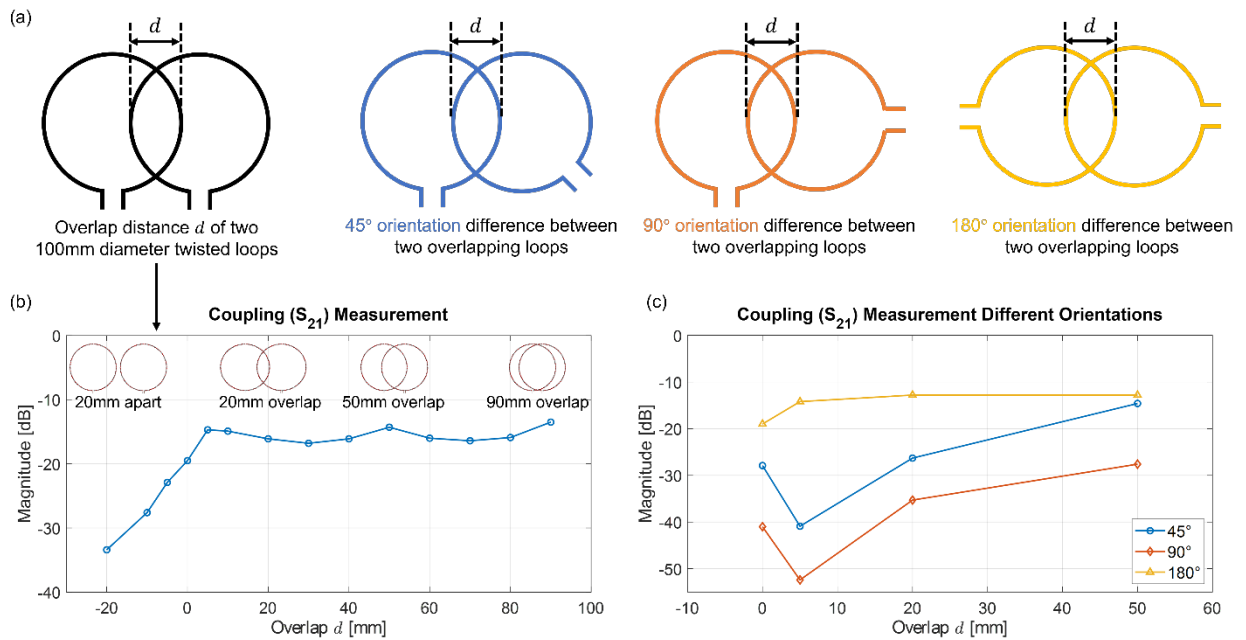


Fig. 6 Coupling results (S_{21}), in dB, of two twisted pair loops for a varying amount of overlap d , in mm. (a) Graphical representation of the different coupling orientations. (b) Coupling results of two loop next to each other. (c) Coupling results for different orientations of the loops, as indicated in (a).

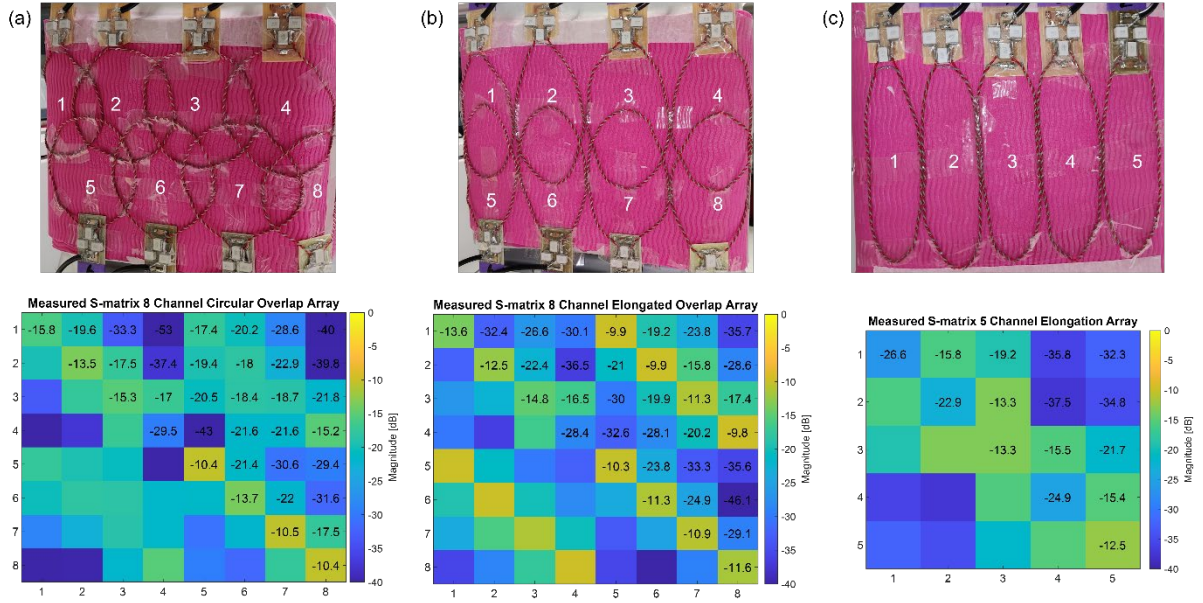


Fig. 7 Measured S-matrices, in dB, for multiple twisted pair coil coupling layouts: (a) 8 channel circular overlap; (b) 8 channel elongated overlap; (c) 5 channel elongated array.

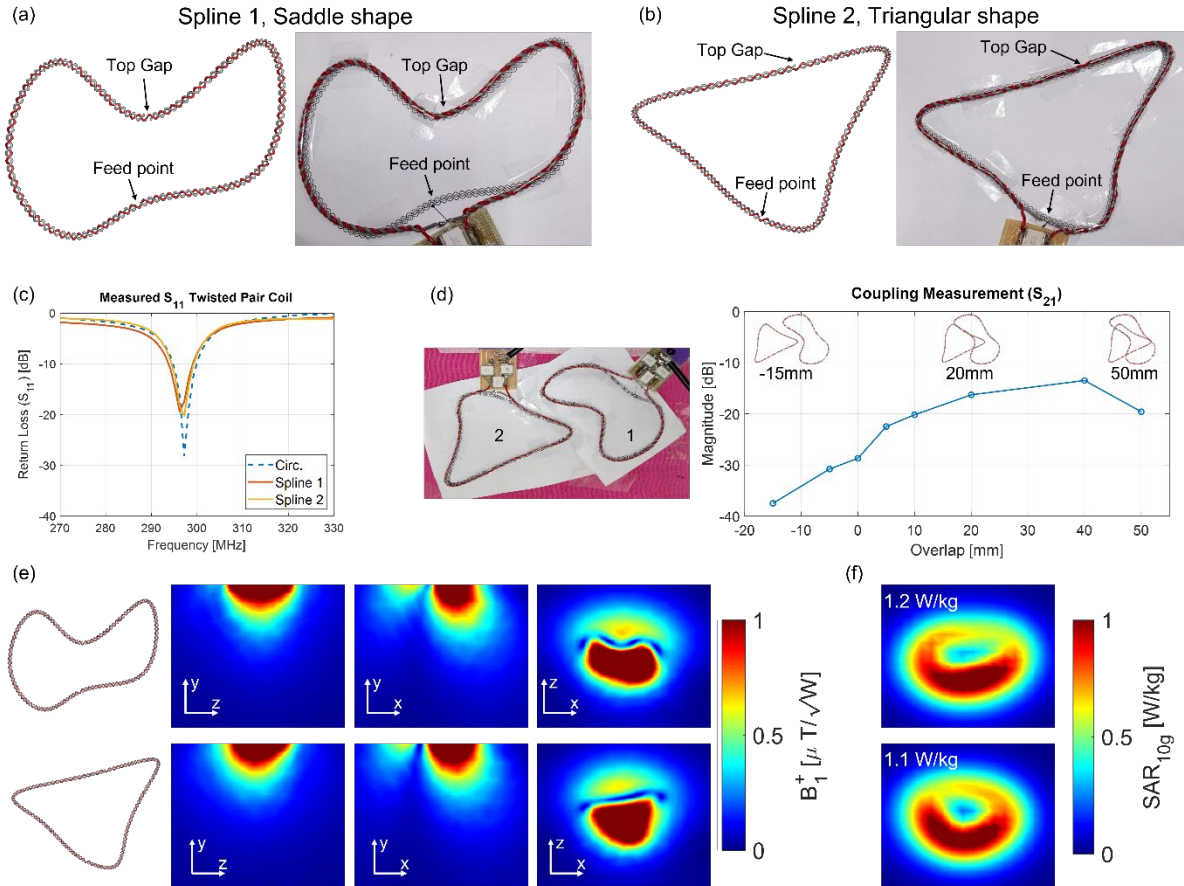


Fig. 8 Different metrics for two realised spline shapes, (a) the **Saddle** and (b) the **Triangle**. (c) Measured return loss (S_{11}), in dB, for both splines and a circular twisted pair coil. (d) Coupling (S_{21}) between the splines for varying amount of overlap. (e) Simulated B_1^+ maps, in $\mu T/\sqrt{W}$, and (f) SAR maps, in W/kg, on the coronal plane with is corresponding peak SAR value. Simulated results were normalised to 1 W accepted power.